CrossMark

Low Surface Brightness Galaxies Selected by Different Model Fitting

Bing-Qing Zhang[1,2], Hong Wu[1,2,3], Wei Du[1], Pin-Song Zhao[1], Min He[1], and Feng-Jie Lei[1]
[1] Key Laboratory of Optical Astronomy, National Astronomical Observatories, Chinese Academy of Sciences, Beijing 100101, China; hwu@bao.ac.cn, bqzhang@bao.ac.cn
[2] School of Astronomy and Space Science, University of Chinese Academy of Sciences, Beijing 100049, China

Abstract

We present a study of low surface brightness galaxies (LSBGs) selected by fitting the images for all the galaxies in α.40 SDSS DR7 sample with two kinds of single-component models and two kinds of two-component models (disk+bulge): single exponential, single sérsic, exponential+deVaucular (exp+deV), and exponential+sérsic (exp +ser). Under the criteria of the B band disk central surface brightness $\mu_{0,\mathrm{disk}}(B) \geqslant 22.5$ mag arcsec^{-2} and the axis ratio $b/a > 0.3$, we selected four none-edge-on LSBG samples from each of the models which contain 1105, 1038, 207, and 75 galaxies, respectively. There are 756 galaxies in common between LSBGs selected by exponential and sérsic models, corresponding to 68.42% of LSBGs selected by the exponential model and 72.83% of LSBGs selected by the sérsic model, the rest of the discrepancy is due to the difference in obtaining μ_0 between the exponential and sérsic models. Based on the fitting, in the range of $0.5 \leqslant n \leqslant 1.5$, the relation of μ_0 from two models can be written as $\mu_{0,\mathrm{sérsic}} - \mu_{0,\mathrm{exp}} = -1.34(n - 1)$. The LSBGs selected by disk+bulge models (LSBG_2comps) are more massive than LSBGs selected by single-component models (LSBG_1comp), and also show a larger disk component. Though the bulges in the majority of our LSBG_2comps are not prominent, more than 60% of our LSBG_2comps will not be selected if we adopt a single-component model only. We also identified 31 giant low surface brightness galaxies (gLSBGs) from LSBG_2comps. They are located at the same region in the color–magnitude diagram as other gLSBGs. After we compared different criteria of gLSBGs selection, we find that for gas-rich LSBGs, $M_\star > 10^{10}M_\odot$ is the best to distinguish between gLSBGs and normal LSBGs with bulge.

Key words: catalogs – galaxies: spiral – galaxies: bulges – methods: data analysis – methods: statistical

1. Introduction

Low surface brightness galaxies (LSBGs) are galaxies whose central surface brightness of the disk component is at least one magnitude fainter than the sky brightness (Impey & Bothun 1997). Studies show that the LSBGs are under-evolved because they generally have sparse Hα emission (Pickering et al. 1997; Huang et al. 2014), low star formation rate (SFR), low SFR surface density (van der Hulst et al. 1993; Galaz et al. 2011; Lei et al. 2018, 2019), and low metallicity (McGaugh & Bothun 1994; Liang et al. 2010). They are rich in neutral hydrogen (H I) gas (de Blok et al. 1996; Burkholder et al. 2001; O'Neil 2004; Du et al. 2015), but have little CO molecules (O'Neil et al. 2003; Honey et al. 2018), indicating that they have low efficiency in converting H I gas to H$_2$ molecules (Cao et al. 2017).

LSBGs are mostly late-type disk-dominated galaxies (McGaugh & Bothun 1994; de Blok et al. 1995). O'Neil et al. (1997) show around 80% of the galaxies in their LSBGs sample are well-fitted by an exponential profile. So it is appropriate to fit the LSBGs with a single disk model, many authors have done so (O'Neil et al. 1997; Du et al. 2015). However, McGaugh et al. (1995b) claim that a small but significant subset of LSBGs has B/D ≈ 1 (bulge-to-disk ratio), Pahwa & Saha (2018) show that about 40% of the galaxies in their LSBGs sample have bulges. This kind of LSBGs that have bulges at their center will be lost if only a single disk model is adopted. Then two approaches arose, one is to process a bulge+disk decomposition to get the central surface brightness of the disk component (Pizzella et al. 2008; Pahwa & Saha 2018), and another is to use the average surface brightness within effective radius ($\bar{\mu}_e$) instead of central surface brightness (μ_0) to reduce the effect of luminosity concentration in the galaxy center (Greco et al. 2018; Martin et al. 2019; Tanoglidis et al. 2021). The second approach cannot get detailed information of the disk component, motivating us to search for LSBGs with bulges by using the bulge+disk decomposition method.

In another aspect, the observation technology improved and the wide-field surveys developed a lot in the last two decades, e.g., the Sloan Digital Sky Survey (SDSS; York et al. 2000), the Dark Energy Camera Legacy Survey (DECaLS; Dey et al. 2019), the Arecibo Legacy Fast ALFA survey (ALFALFA;

---

[3] Author to whom any correspondence should be addressed.

Giovanelli et al. 2005). People can dig deeper and wider in the sky, also bringing more opportunities for us to search for LSBGs. For example, 12 282 LSBGs were selected from SDSS data release 4 (DR4) to study their stellar population (Zhong et al. 2008) and metallicities (Liang et al. 2010); Galaz et al. (2011) also selected 9421 LSBGs from SDSS DR4 to investigate their spatial distribution. The combination of optical images and H I spectra provides us with one of the best laboratories for studying gas-rich LSBGs. Haynes et al. (2011) provide a cross-reference catalog, which contains 12468 galaxies, of α.40 (40% sky area of the full ALFALFA) and SDSS Data Release 7 (DR7; Abazajian et al. 2009), and Du et al. (2015) (hereafter Du15) developed a pipeline to reestimate the sky background for 12,423 galaxies belonging to the PhotoPrimary catalog in the α.40 SDSS DR7 sample to avoid the sky background overestimation by the photometric pipeline of the SDSS. Based on the background resubtracted images, Du15 selected a none-edge-on LSBG sample of 1129 galaxies by using a single exponential model fitting, this paper focuses on selecting LSBGs from different models and searching for LSBGs with bulges by applying the disk+bulge model.

The rest of the paper is arranged as follows. In Section 2, we describe our parent sample, model fitting, and the method of central surface brightness (μ_0) calculation. Section 3 shows our LSBG samples and their statistical properties. In Section 4, we discuss the gLSBGs selection. Finally, we summarize this paper in Section 5.

2. Sample and Fitting

2.1. Parent Sample

Many researchers, including the ones in the SDSS team, noticed that the sky background in the SDSS imaging pipeline is overestimated (Adelman-McCarthy et al. 2006, 2008; Lauer et al. 2007; Liu et al. 2008; Hyde & Bernardi 2009; He et al. 2013), leading to the galaxy brightness being underestimated. Because the central surface brightness of LSBGs is fainter than the sky background, the outer parts of LSBGs are even fainter. The inaccurate background will influence the photometry, model fitting, and LSBG selection. Du15 carefully estimated the sky background of SDSS images in both g and r bands for 12,423 galaxies in the α.40 SDSS DR7 sample (Haynes et al. 2011). After their background subtraction, the count distributions for the whole image and the local vicinity, which defined as the region between the two square boxes sized 250×250 pixels and 500×500 pixels from the galaxy center, are both well fitted by a Gaussian profile with mean values very close to 0 ADU (see Figure 3 in Du15). We take the 12,423 galaxies as our parent sample in selecting LSBGs, taking advantage of their better analysis on the sky subtraction.

We took photometry for all galaxies in our parent sample by using SExtractor software (Bertin & Arnouts 1996). A flexible

elliptical aperture, the Kron aperture defined by Kron (1980), was used to get magnitude (MAG_AUTO). The apertures of g and r bands are the same which were defined by the r band image. The parameters from SExtractor, including magnitude, effective radius, axis ratio, and position angle, are used as the initial guess for model fitting.

2.2. Model Fitting

Galfit is a two-dimensional fitting algorithm to extract structural components of galaxies (Peng et al. 2002, 2010). It provides some of the most commonly used radial profiles in astronomy literature, e.g., the exponential, sérsic, deVaucular, Gaussian, moffat, and psf profiles. The exponential and deVaucular profiles are special cases of the sérsic function when $n = 1$ and $n = 4$, respectively. Users can adopt a single profile or a combination of a number of profiles, and set initial values for input parameters of each profile. During the fitting, the reduced χ^2 is minimized, and the minimization engine is based on the Levenberg-Marquardt downhill gradient algorithm.

We carried out two kinds of single-component fitting and two kinds of two-component (disk+bulge) fitting: the single exponential profile, the single sérsic profile, combination of the exponential and deVaucular profile (hereafter, exp+deV), and combination of the exponential and sérsic profile (hereafter, exp+ser). Since most galaxies in our parent sample can be fully shown in 501×501 pixels, all the fittings are performed in this region with the target located at the center to improve Galfit fitting efficiency. During fitting, a psf image and mask image were used to get better results. The psf images were derived from SDSS website (http://das.sdss.org/imaging) to describe the local psf profile surrounding the target, and the mask images were produced on the basis of the segmentation image from SExtractor. We masked out other objects, only the background and target regions are fitted.

We also set limitations on a variable range of parameters to avoid unphysical fittings. For all the models and subcomponents, the variable range of the galaxy center is ± 5 pixels in both horizontal and vertical directions. Based on the assumption that half of the diagonal size of our images (~ 354 pixel) being exactly three times the R_e of the galaxy, we set the variable range of the effective radius (R_e) as $1 \sim 118$ pixels, that is $1 \leqslant R_e \leqslant 118$ for sérsic and deVaucular profile and $1 \leqslant 1.678 \times R_s \leqslant 118$ for the exponential profile, where R_s is the scale length. Here we use R_s instead of R_e for the exponential profile because the exponential profile provided by Galfit (Equation (1)) uses R_s, and there is a relation between R_e and R_s for the exponential profile, $R_e = 1.678 \times R_s$ (Peng et al. 2010, Equation (7)]. For the sérsic model, the variable range of the n index is $0.5 \sim 8.0$, which is the same range as Simard et al. (2011). When $n < 0.5$, the luminosity density of the sérsic profile has a depression in its center, which is often unphysical (see Trujillo et al. 2001, Figure 6). For the exp+ser model, the

Table 1
Sample Numbers after each Step

	exponential		sérsic		exp+deV		exp+ser	
	g	r	g	r	g	r	g	r
feed in Galfit[a]	12423	12423	12423	12423	5233	5233	5233	5233
have Galfit output	12218	12218	12217	12217	4560	4665	4461	4680
numerical reasonable[b]	12058	12088	11096	11353	3592	3800	2045	2379
good structure parameters[c]	11697		10582		3031		1495	
$R_{e,\mathrm{disk}} > R_{e,\mathrm{bulge}}$	⋯		⋯		1981		1066	
well-fitted sample	11697		10582		1981		1066	
LSBG sample (initial)	1151		1081		286		175	
LSBG sample (after visual inspection)	1105		1038		207		132	
LSBG sample ($n_b > 1.5$)[d]	⋯		⋯		⋯		75	

Notes.
[a] The number of galaxies that we feed in Galfit for exp+deV and exp+ser fitting excludes the galaxies that satisfy $0.5 \leqslant n \leqslant 1.5$ for both g and r bands in sérsic fitting.
[b] The numerical reasonable fittings are fittings whose R_e, R_s, and n index do not reach the boundaries.
[c] The structure parameters mean the axis ratio (b/a) and position angle (PA). We calculate the difference between g and r bands and execute a 3σ clipping, for b/a and PA one by one. The fittings with good structure parameters mean their b/a and PA are consistent between the g and r bands.
[d] The n_b represents the n index of bulge component.

variable range of the n index of the sérsic component is $1.0 \sim 8.0$, here we force the bulge component (sérsic) to be more concentrated than the disk component (exponential) by applying a larger n value of the sérsic profile than that of the exponential profile.

Note that all the galaxies have been fitted with the exponential and the sérsic profile, then 5233 galaxies (42.12% of parent sample) were selected to run the disk+bulge model fitting by eliminating 7190 galaxies whose sérsic n index $0.5 \leqslant n \leqslant 1.5$ for both g and r bands. This is because, for disk-dominated galaxies, the application of a disk+bulge model by force would lead Galfit to converge to no results.

After fitting, we took the following steps to filter the fitting results:

1. Eliminate numerical unreasonable fittings. When numerical convergence issues happen during fitting, the entire solution is not reliable, we will remove the galaxy from further analysis. The galaxy will also be removed if the output parameters reach the boundaries we set. In this step, for sérsic and exp+ser models, most of the removed galaxies are because their fitted n index are at the boundary values.
2. Eliminate fitting results whose structure parameters, such as the axis ratio (b/a) and position angle (PA), are not consistent between the g and r bands. For b/a and PA, we calculate the difference for all the galaxies and execute a 3σ clipping.
3. For disk+bulge fitting, galaxies will be removed if their fitted effective radius of the disk component is smaller than those of the bulge component.

After these steps, we constructed four "well-fitted" samples which contain 11 697, 10 582, 1981, and 1066 galaxies for exponential, sérsic, exp+deV, and exp+ser model fitting, respectively. The galaxies in the "well-fitted" samples have good fitting results in both g and r bands, and will be used in the following analysis. The numbers of galaxies after each step are listed in Table 1.

2.3. The Central Surface Brightness

In the following, we will illustrate the procedures of how we calculate μ_0 for the exponential profile and the sérsic profile step by step.

The expression of the exponential profile is:

$$f(r) = f_0 \exp\left(-\frac{r}{r_s}\right). \tag{1}$$

The flux integrated out to $r = \infty$ is:

$$F_{\mathrm{total}} = 2\pi r_s^2 f_0 q \tag{2}$$
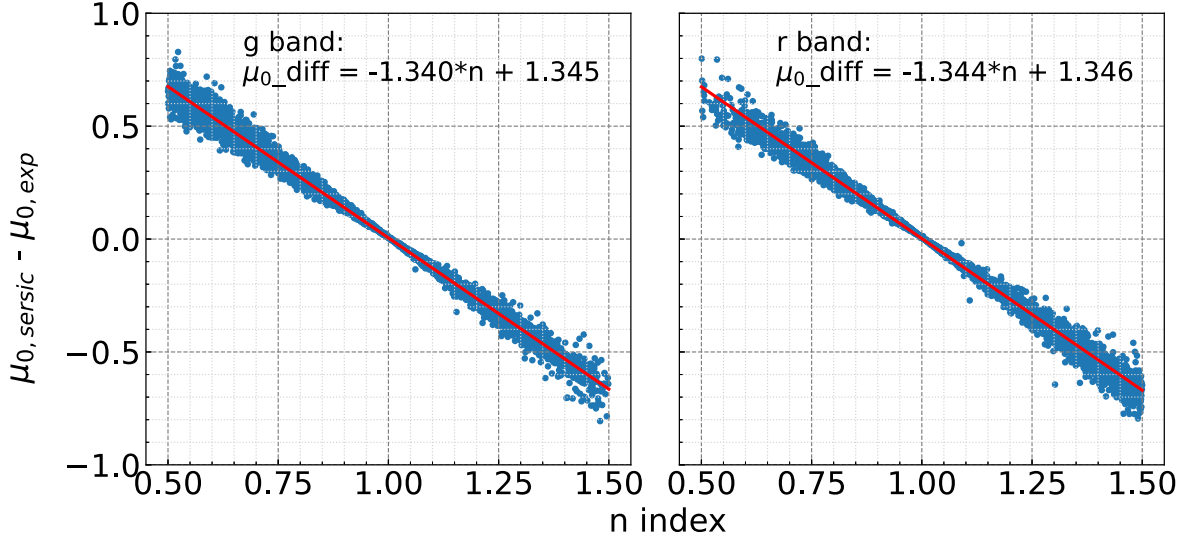
where q is the axis ratio.

So the central surface brightness can be expressed as:

$$f_0 = \frac{F_{\mathrm{total}}}{2\pi r_s^2 q}. \tag{3}$$

Then, apply cosmological dimming correction, also convert the unit of f_0 to mag arcsec^{-2}, the central surface brightness is:

$$
\begin{aligned}
\mu_0 &= -2.5 \log_{10}(f_0) - 10 \log_{10}(1 + z) \\
&= m + 2.5 \log_{10}(2\pi r_s^2 q) - 10 \log_{10}(1 + z)
\end{aligned} \tag{4}
$$

where m is the model magnitude, r_s is the disk scale length, and z is from $\alpha.40$ catalog.

Figure 1. The relation between the difference of central surface brightness from exponential and sérsic fitting and the sérsic n index. The red solid lines are the linear fitting of the points. The fitting functions are written on the top of each panel.

For the sérsic model, the function is:

$$f(r) = f_e \exp\left[-\kappa\left(\left(\frac{r}{r_e}\right)^{\frac{1}{n}} - 1\right)\right]. \tag{5}$$

The flux integrated out to $r = \infty$ is:

$$F_{\text{total}} = 2\pi r_e^2 f_e \, e^\kappa n\kappa^{-2n}\Gamma(2n)q. \tag{6}$$

So the surface brightness at the effective radius(f_e) and galaxy center(f_0) is:

$$f_e = \frac{F_{\text{total}}}{2\pi r_e^2 e^\kappa n\kappa^{-2n}\Gamma(2n)q} \tag{7}$$

$$f_0 = f_e \, exp(\kappa) = \frac{F_{\text{total}}}{2\pi r_e^2 n\kappa^{-2n}\Gamma(2n)q} \tag{8}$$

where r_e is the effective radius, n is the sérsic index, κ is related to n index $\kappa = 1.9992n - 0.3271$ (Capaccioli 1989), Γ function is $\Gamma(2n) = (2n - 1)!$.

Then, apply cosmological dimming correction, also convert the unit of f_0 to mag arcsec^{-2}, the central surface brightness is:

$$\begin{aligned}\mu_0 &= -2.5 \log_{10}(f_0) - 10 \log_{10}(1 + z) \\ &= m + 2.5 \log_{10}(2\pi r_e^2 n\kappa^{-2n}\Gamma(2n)q) - 10 \log_{10}(1 + z).\end{aligned} \tag{9}$$

Finally, the B band central surface brightness can be transferred by an empirical equation (Smith et al. 2002):

$$\mu_0(B) = \mu_0(g) + 0.47(\mu_0(g) - \mu_0(r)) + 0.17. \tag{10}$$

Figure 1 shows the difference of μ_0 between exponential and sérsic fitting varies with sérsic n index for galaxies which have $0.5 \leqslant n \leqslant 1.5$ in both g and r bands. The red solid lines are the

linear fitting of the points, which can be described as follows:

$$g \text{ band: } \mu_{0,\text{sérsic}} - \mu_{0,\text{exp}} = -1.340n + 1.345 \tag{11}$$

$$r \text{ band: } \mu_{0,\text{sérsic}} - \mu_{0,\text{exp}} = -1.344n + 1.346 \tag{12}$$

which also be written on the top of each panel. The expression can be simplified to

$$\mu_{0,\text{sérsic}} - \mu_{0,\text{exp}} = -1.34(n - 1). \tag{13}$$

The relationship between μ_0 difference and n index distributes along a biconical shape, which is best when $n = 1$, and becomes worse with the increase or decrease of n index. When $n > 1$, the μ_0 obtained from the sérsic model is brighter than that from the exponential model, and when $n < 1$, the μ_0 obtained from the sérsic model is dimmer than that from the exponential model. The two models yield a μ_0 difference of up to approximately 0.7 mag arcsec^{-2}.

3. LSBG Samples

3.1. LSBG Selection

There has been no consensus in the threshold values of μ_0 to define LSBGs, people apply different cut in literature ($\mu_{0,\text{disk}}(B) = 22.0$ mag arcsec^{-2} (McGaugh et al. 1995a), 22.5 mag arcsec^{-2} (McGaugh 1996; Rosenbaum et al. 2009; Du15), 23.0 mag arcsec^{-2} (Impey & Bothun 1997); $\mu_{0,\text{disk}}(V)$ =21.2 mag arcsec^{-2} (Brown et al. 2001); $\mu_{0,\text{disk}}(R) =$ 20.8 mag arcsec^{-2} (Courteau 1996; Brown et al. 2001); $\mu_{0,\text{disk}}(r) = 21.0$ mag arcsec^{-2} (Pahwa & Saha 2018)). In this paper, we adopt a threshold of $\mu_{0,\text{disk}}(B) \geqslant 22.5$ mag arcsec^{-2} and apply $b/a \geqslant 0.3$ to avoid the internal extinction effect (He et al. 2020).
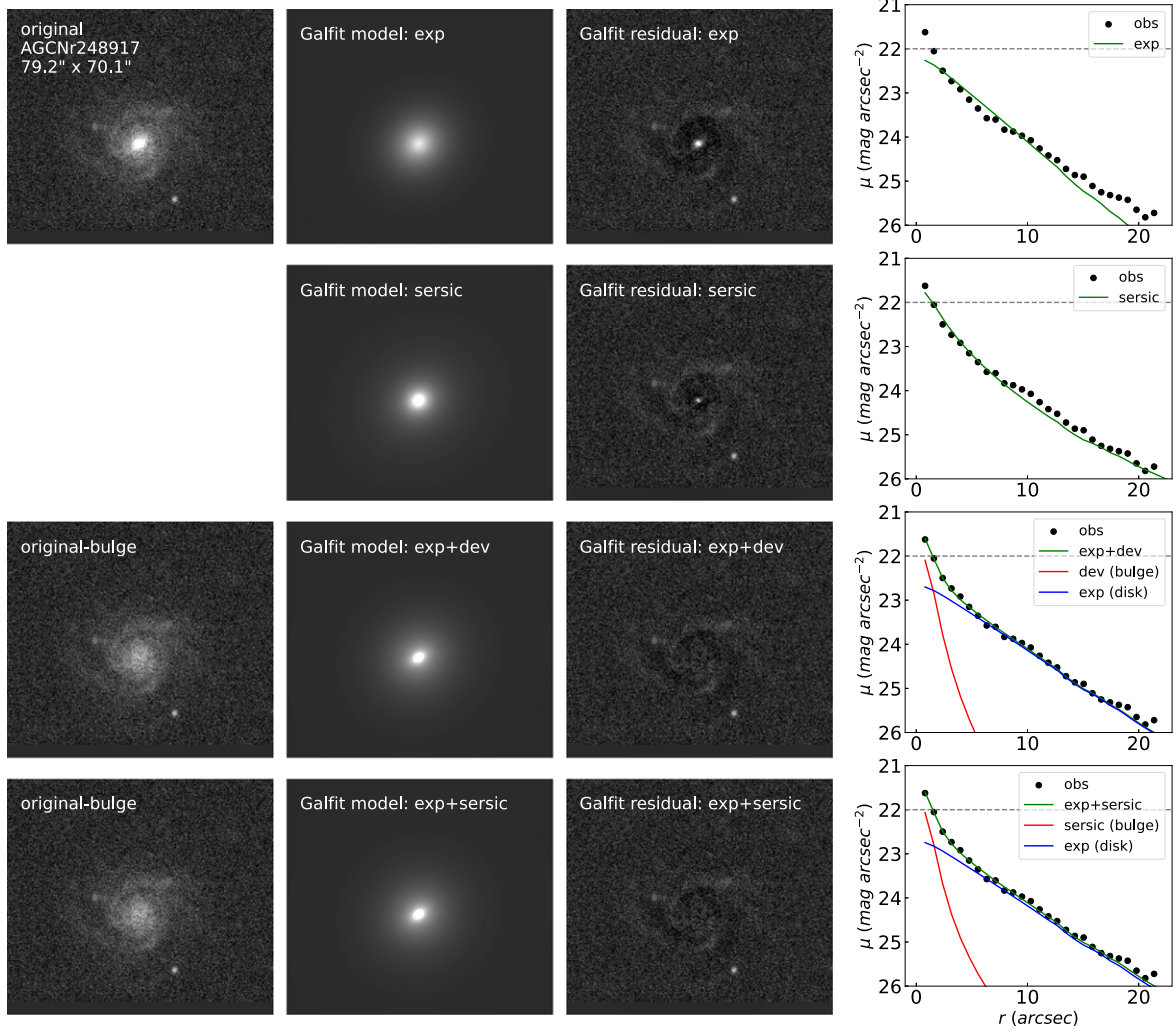
Figure 2. An example of Galfit fitting results of four models, exponential, sérsic, exp+deV, and exp+ser, from top to bottom. This galaxy is selected as LSBG by "exp+deV" and "exp+ser" models. The upper left corner shows the observed image, the second column shows the model images, the third column shows the residual images (observed image minus model image), and the fourth column is the radial distribution of surface brightness obtained from a series of elliptical annulus on the observed image and models, with a step of 2 pixels. The bottom two rows of the first column show the pure disk image (observed image minus bulge component).

With this selection criterion, and the visual inspection afterwards, we selected four LSBG samples from the "well-fitted sample" of each model: LSBG_exp, LSBG_sérsic, LSBG_exp+deV, and LSBG_exp+ser, which contain 1105 galaxies (9.45% of "exponential" well-fitted sample), 1038 galaxies (9.81% of "sérsic" well-fitted sample), 207 galaxies (10.45% of "exp+deV" well-fitted sample), and 132 galaxies (12.38% of "exp+ser" well-fitted sample). During the visual inspection, fittings were deleted if the model was influenced obviously by the neighbors or the galaxy is peculiar in morphology. Considering that our original intention was to look for LSBGs with bulge, we set a limitation on the n index of bulge component of "exp+ser" model $n_b > 1.5$ to exclude some "disk+disk" fitting results, and there are 75 LSBGs satisfy this criterion in both g and r bands. The galaxy numbers

of initial LSBG samples and final LSBG samples are listed in Table 1. The table containing all the parameters of our LSBGs (DOI: 10.57760/sciencedb.13130) is available in its entirety in a machine-readable form in the Science Data Bank database, the column descriptions are listed in Table 2.

For the LSBGs selected from two-component fitting, the two-component fitting is usually better than the one-component fitting. Figure 2 shows an example of Galfit fitting results (AGCNr 248 917) of our four models, exponential, sérsic, exp+deV, and exp+ser, from top to bottom. This galaxy is selected as LSBG by "exp+deV" and "exp+ser" models. The first image in the upper left panel shows the observed image, the second column shows the model images, the third column shows the residual images (observed image minus model image), and the fourth column is the radial distribution of surface brightness

Table 2
Column Descriptions of our LSBG Table

| Column name	Description	Unit
note	Model adopt	
AGCNr	ID in $\alpha.40$ catalog	
R.A.	Right ascension (J2000.0)	degree
decl.	decl. (J2000.0)	degree
Vhelio	Heliocentric velocity of the HI profile midpoint from $\alpha.40$ catalog	km s^{-1}
Dist	Distance from $\alpha.40$ catalog	Mpc
logMHI	HI mass from $\alpha.40$ catalog	logarithmic solar mass
W50	Observed velocity width at 50% of peak on either side from $\alpha.40$ catalog	km s^{-1}
kpc_per_arcsec	image scale factor	kpc arcsec^{-1}
kpc_per_pix	image scale factor	kpc pixel^{-1}
magauto_all_band	Magnitude for the whole galaxy from SExtractor	mag
magautoerr_all_band	Error of magnitude for the whole galaxy from SExtractor	mag
MAG_obs_band	Absolute magnitude for the whole galaxy	mag
M_star_obs_band	Stellar mass for the whole galaxy	logarithmic solar mass
mag_disk_band	Magnitude of disk component from model fitting	mag
mag_disk_err_band	Error of magnitude of disk component from model fitting	mag
rs_disk_band	Disk-scale length of disk component from model fitting	pixel
rs_disk_err_band	Error of disk-scale length of disk component from model fitting	pixel
re_disk_band	Effective radius of disk component from model fitting	pixel
re_disk_err_band	Error of effective radius of disk component from model fitting	pixel
n_disk_band	sérsic n index of disk component from model fitting	
n_disk_err_band	Error of sérsic n index of disk component from model fitting	
ar_disk_band	Axis ratio of disk component from model fitting	
ar_disk_err_band	Error of axis ratio of disk component from model fitting	
pa_disk_band	Position angle of disk component from model fitting	degree: Up = 0 Left = 90
pa_disk_err_band	Error of position angle of disk component from model fitting	degree: Up = 0Left = 90
mag_bulge_band	Magnitude of bulge component from model fitting	mag
mag_bulge_err_band	Error of magnitude of bulge component from model fitting	mag
re_bulge_band	Effective radius of bulge component from model fitting	pixel
re_bulge_err_band	Error of effective radius of bulge component from model fitting	pixel
n_bulge_band	sérsic n index of bulge component from model fitting	
n_bulge_err_band	Error of sérsic n index of bulge component from model fitting	
ar_bulge_band	Axis ratio of bulge component from model fitting	
ar_bulge_err_band	Error of axis ratio of bulge component from model fitting	degree: Up = 0 Left = 90
pa_bulge_band	Position angle of bulge component from model fitting	degree: Up = 0 Left = 90
pa_bulge_err_band	Error of position angle of bulge component from model fitting	
mu0_disk_band	Central surface brightness of disk component	mag arcsec^{-2}
mu0_disk_err_band	Error of central surface brightness of disk component	mag arcsec^{-2}
B/T_band	Bulge-to-total ratio from model fitting	

Note. This is column descriptions of our LSBG table. The related table (DOI: 10.57760/sciencedb.13130) is available in its entirety in a machine-readable form in the Science Data Bank database.

obtained from a series of elliptical annulus on the observed image and models, with a step of 2 pixels. The pure disk image is also displayed in the bottom two rows of the first column by using the observed image minus the bulge component. From the residual image of exponential and sérsic fitting, it is obvious that there is a small bright spot in the galaxy center, and this small bright spot can be fitted well by exp+deV and exp+ser models.

3.2. Statistical Properties of LSBG Samples

Figure 3 shows the statistical properties of our four LSBG samples: panels (a) and (b) show the distribution of the B band central surface brightness ($\mu_{0,\mathrm{disk}}(B)$) and g band effective radius ($R_{e,\mathrm{disk}}(g)$) of the disk component; panels (c)$\sim$(g) show the distribution of $g - r$ color, g band absolute magnitude (M_g), g band stellar mass ($\log(M_\star/M_\odot)(g)$), H I gas mass ($\log(M_{\mathrm{H\,I}}/M_\odot)$), and H I line width (W50) for the whole galaxy. The H I gas mass and W50 are from the $\alpha.40$ catalog (Haynes et al. 2011). The stellar mass was calculated by using the prescription in Du et al. (2020). In that, we compute mass-to-light ratio by using the $g - r$ color: $\log_{10}(M/L)_\lambda = a_\lambda + (b_\lambda \times (g - r))$, where $a_g = -0.857$, $b_g = 1.558$, $a_r = -0.7$, and $b_r = 1.252$. The absolute magnitude was calculated by using the distance from the $\alpha.40$ catalog by adopting $H_0 = 70\,\mathrm{km\ s^{-1}Mpc^{-1}}$ (Haynes et al. 2011), and the absolute
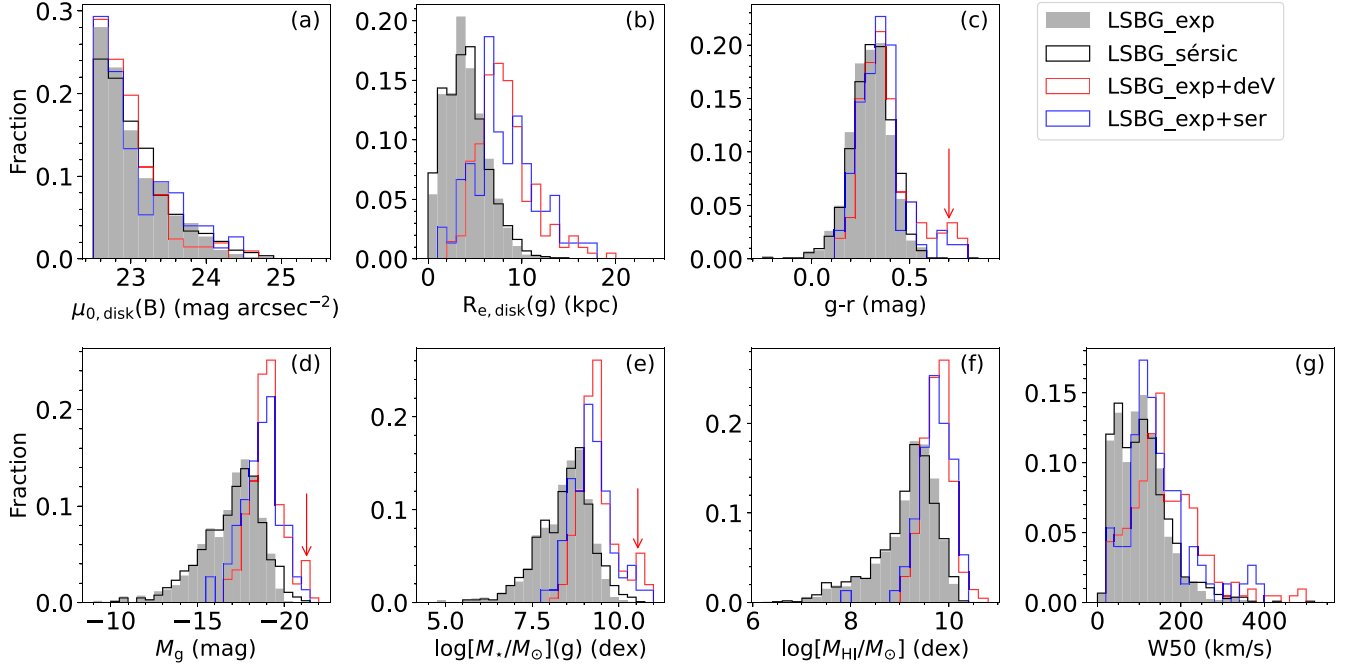
Figure 3. The statistical properties of our four LSBG samples. The B band central surface brightness ($\mu_{0,\text{disk}}(B)$) and g band effective radius ($R_{e,\text{disk}}(g)$) of the disk component are from model fitting; the $g - r$ color, g band absolute magnitude (M_g), and g band stellar mass ($\log(M_\star/M_\odot)(g)$) are from photometry; the H I gas mass and W50 are from the α.40 catalog (Haynes et al. 2011). The red arrows in panels (c), (d), and (e) point out another peak of distributions of LSBG_exp+deV and LSBG_exp+ser samples.

Table 3
The Median Values of Parameters of our Four LSBG Samples

	$\mu_{0,\text{disk}}(B)$ (mag arcsec^{-2})	$R_{e,\text{disk}}(g)$ (kpc)	$g - r$ (mag)	M_g (mag)	$\log(M_\star/M_\odot)(g)$ ($M_\odot$)	$\log(M_{\text{H I}}/M_\odot)$ ($M_\odot$)	W50 (km s^{-1})
LSBG_exp	22.888	3.843	0.298	−17.257	8.539	9.28	100.0
LSBG_sérsic	22.936	3.840	0.311	−17.294	8.561	9.25	100.0
LSBG_exp+deV	22.882	7.902	0.354	−18.965	9.305	9.76	149.0
LSBG_exp+ser	22.897	7.665	0.343	−18.774	9.195	9.72	127.0

magnitude of the Sun is $M_{g,\odot} = 5.11$ and $M_{r,\odot} = 4.65$ (Willmer 2018). We list the median values of these parameters of our four LSBG samples in Table 3. Table 4 lists the number statistics of the overlapping galaxies that are both selected as LSBGs in any of the two LSBG samples.

3.2.1. Comparison of LSBG_exp and LSBG_sérsic

It is obvious to see that all the parameters of LSBG_exp (the gray filled histograms) and LSBG_sérsic (the black steps) have very similar distributions, and the median values of these parameters are close. Figure 4 shows the distribution of n index of galaxies in LSBG_sérsic, 97.40% (1011/1038) of the galaxies have $0.5 < n < 1.5$ for g band and 91.62% (951/1038) for r band, indicating our LSBGs selected by sérsic fitting are in principle the same type of galaxies as those selected by exponential fitting. These two samples have 756 galaxies (68.42% of LSBG_exp and 72.83% of LSBG_sérsic) in

common, the rest of the discrepancy is due to the difference in obtaining μ_0 between the two models as we mentioned in Section 2.3. That is, the remaining galaxies have μ_0 brighter than 22.5 mag arcsec^{-2} in one fitting result and dimmer than 22.5 mag arcsec^{-2} in the other fitting result.

3.2.2. Comparison of LSBG_exp+deV and LSBG_exp+ser

The distributions of all the parameters of the galaxies in LSBG_exp+deV (the red steps) and LSBG_exp+ser (the blue steps) are also similar, but the median values of these parameters of LSBG_exp+deV are slightly larger than those of LSBG_exp+ser.

Fisher & Drory (2008) found that the sérsic index of bulge can be used to distinguish between classical and pseudo bulges: classical bulges have $n_b \gtrsim 2$ and pseudo bulges have $n_b \lesssim 2$ in the V band with almost no overlap. Considering that the g band has more similar wavelength coverage to the V band than the r

Table 4
The Numbers of Galaxies Duplicated in any Two LSBG Samples

	LSBG_exp	LSBG_sérsic	LSBG_exp+deV	LSBG_exp+ser	LSBG_exp+ser ($n > 2$)
LSBG_exp	1105	756	76	28	13
LSBG_sérsic	756	1038	15	4	0
LSBG_exp+deV	76	15	207	35	22
LSBG_exp+ser	28	4	35	75	37
LSBG_exp+ser ($n > 2$)	13	0	22	37	37
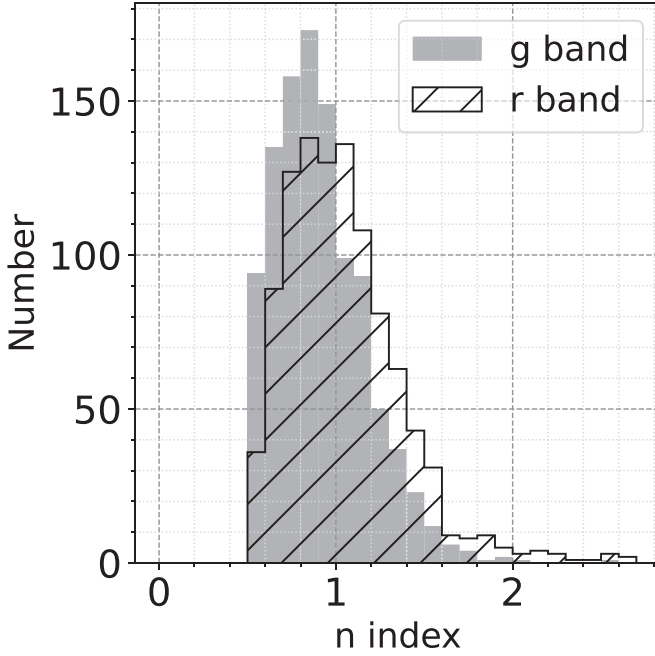
Figure 4. The distribution of n index for galaxies in LSBG_sérsic. Around 97.40% of them have $0.5 < n_g < 1.5$ and 91.62% have $0.5 < n_r < 1.5$.

band, we divide the bulges in the LSBG_exp+ser sample into classical and pseudo bulges according to their n index of bulge component (n_b) in the g band. Of these 75 galaxies, 50 galaxies are classified as galaxies with classical bulges.

Among the 50 LSBGs that hold classical bulges, 24 of them are selected as LSBGs by "exp+deV" fitting. In the rest 26 galaxies in LSBG_exp+ser, 25 of them are not in the "exp+deV" well-fitted sample, only one galaxy (AGCNr 102 234) is in but not selected as LSBG because it does not satisfy the $b/a \geqslant 0.3$ criterion. The reason why one model can get the fitting result but the other model cannot is beyond the scope of this paper. Only considering the galaxies that both models can get good fitting results, almost all the LSBGs with classical bulges selected by the "exp+ser" model can be selected by the "exp+deV" model.

### 3.2.3. Comparison of LSBGs Selected by One-component and Two-component Fitting

For convenience, we will call the galaxies in LSBG_exp and LSBG_sérsic "LSBG_1comp" (in total 1387 galaxies),

and the galaxies in LSBG_exp+deV and LSBG_exp+ser "LSBG_2comps" (in total 247 galaxies). There are in total 1546 LSBGs with 88 duplicating in LSBG_1comp and LSBG_2comps, suggesting 15.98% (247/1546) of our LSBGs hold bulge. It should be noted that this fraction might be smaller than it actually is, since we perform two-component fitting only for galaxies with $n > 1.5$ in the single sérsic fitting, as a result, some galaxies with small bulges will be missed. Among the 88 overlapped galaxies of LSBG_1comp and LSBG_2comps, 96.59% (85/88) of them have B/T < 0.25, as a blue histogram in Figure 7(c) shown, suggesting that the 88 overlapped LSBGs have small bulges, they can be fitted well by a single component model. The remaining 1299 galaxies in LSBG_1comp can be considered as a single disk without bulges. Even if they do contain a bulge, the B/T would be smaller than that of the overlaps.

The median values of $R_{e,\text{disk}}$, g band stellar mass, H I mass, and W50 of LSBG_2comps are $3.8 \sim 4.1$ kpc, $0.63 \sim 0.76$ dex, $0.44 \sim 0.52$ dex, and $30 \sim 50$ km s^{-1} larger than those of LSBG_1comp, the median value of g band absolute magnitude of LSBG_2comps is about $1.5 \sim 1.7$ mag brighter than that of LSBG_1comp. Compared to LSBG_1comp, the distributions of LSBG_exp+deV and LSBG_exp+ser have another peak at the red and massive (or bright) end, we point out the peaks in panels (c), (d), and (e) in Figure 3 by red arrows, the giant low surface brightness galaxies (gLSBGs) contribute a lot to this peak. However, the median value of $g - r$ color distribution of LSBG_2comps is only $0.03 \sim 0.05$ mag redder than that of LSBG_1comp, and this is because the bulges are not prominent in the majority of our LSBG_2comps. The distribution of bulge-to-total ratio (hereafter, B/T) shown in Figure 5 shows 82.61% (171/207) of the galaxies in LSBG_exp+deV and 77.33% (58/75) the galaxies in LSBG_exp+ser have B/T < 0.3.

Figure 6 shows the stellar mass distribution of our parent sample and galaxies that fitted by two-component models. The histogram is normalized by its peak value. We can see that the galaxies selected for two-component fitting are indeed the more massive galaxies in the parent sample, and the fraction of selected galaxies in each mass bin increases with the increase in stellar mass. This suggests that the result we obtained that the g-band stellar mass of the LSBG_2comps is $0.63 \sim 0.76$ dex
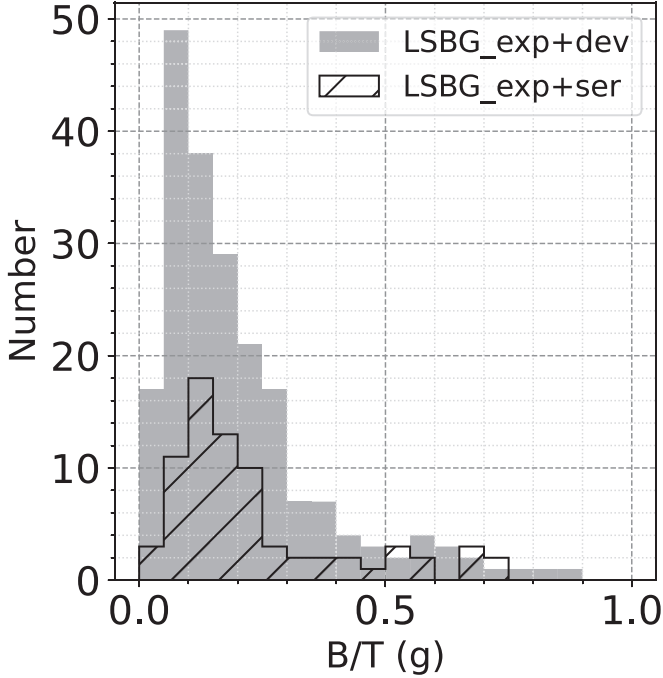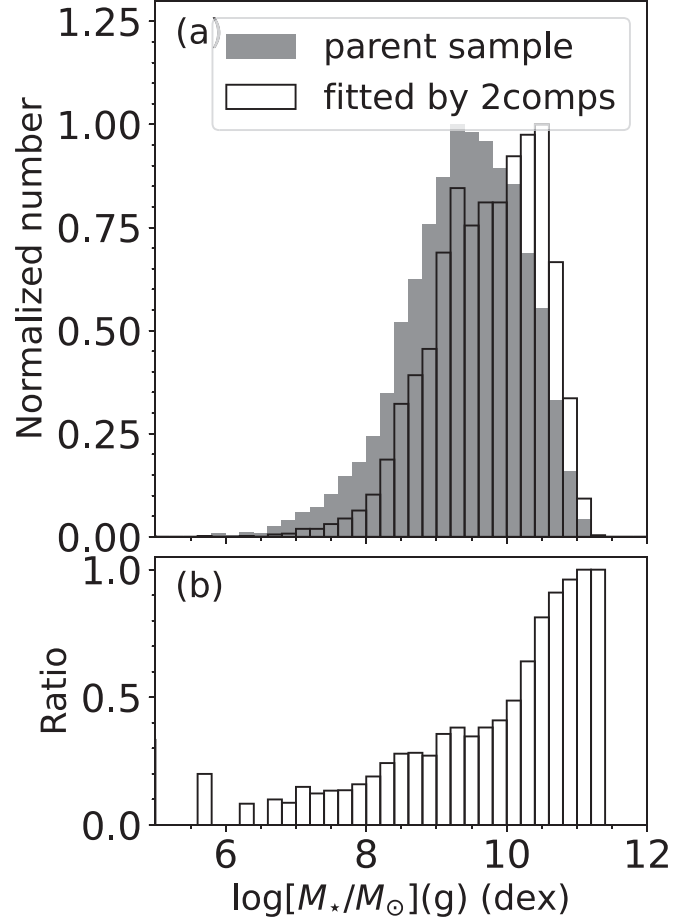
Figure 5. The distribution of *g* band bulge-to-total ratio (B/T) of galaxies in LSBG_exp+deV and LSBG_exp+ser. Around 82.61% of the galaxies in LSBG_exp+deV and 77.33% in LSBG_exp+sérsic have B/T < 0.3.


Figure 6. (a) The histograms of *g* band stellar mass of our parent sample and galaxies fitted by two-component models. The histogram is normalized by its peak value. (b) The label of *y*-axis is the ratio of galaxy number that fitted by two-component models and galaxy number of our parent sample.

larger than that of the LSBG_1comp is partly due to the selection effect. However, we think part of the result reflects the true differences of LSBG_2comps and LSBG_1comp: the disk component in "disk+bulge" LSBGs is larger than that in single disk LSBGs (Figure 3(b)), larger size often corresponds to larger mass. Moreover, the presence of bulge also contributes to the stellar mass observed in the LSBG_2comps.

3.2.4. Loss Fraction of LSBGs with Bulges

Among our LSBG_2comps, about 35.63% (88/247) of them were also identified as LSBGs by single-component fitting (blue circles in Figure 7, denoted as "also LSBG_1comp"), 61.13% (151/247) were not identified as LSBGs by single-component fitting (red circles in Figure 7, denoted as "not LSBG_1comp"), and 3.24% (8/247) do not have good single-component fitting results because they were deleted in the second step of fitting results filtering (see Section 2.2). That is, more than 60% of the LSBG_2comps will not be selected if we adopt a single disk model only. The $\mu_{0,\mathrm{disk}}$ of two-component fitting is dimmer than that of single-component fitting, and the μ_0 difference is related to the B/T of the galaxy. 72.47% (179/247) of our LSBG_2comps have B/T ⩽ 0.2, and in this range the single-component fitting will result in an overestimation of the μ_0 by approximately 0.8 mag arcsec^{-2}.

4. Giant Low Surface Brightness Galaxies

Giant low surface brightness galaxies (gLSBGs) are a subset of LSBGs, they could have comparable or larger mass comparing with the Milky Way, but several times the size of the Milky Way. One of the most well-known gLSBG, Malin 1, was discovered by Bothun et al. (1987). Subsequent studies show Malin 1 has H I mass $M_{\mathrm{H\,I}} \sim 10^{11} M_\odot$ (Bothun et al. 1987), disk central surface brightness $\mu_{0,\mathrm{disk}}(R) = 24.7$ mag arcsec^{-2} (for h = 0.7; Moore & Parker 2006), and its optical diameter can reach 160 kpc (Galaz et al. 2015). UGC 1382 is also a very large gLSBG whose effective radius is 38 kpc (Hagen et al. 2016). But gLSBGs whose size comparable with Malin 1 and UGC 1382 are rare, most of the gLSBGs have scale length from a few kpc to dozens of kpc (McGaugh & Bothun 1994; Sprayberry et al. 1995; H18; S23).

In Table 5, we list different criteria used to select gLSBGs in previous works. In general, there are roughly three kinds
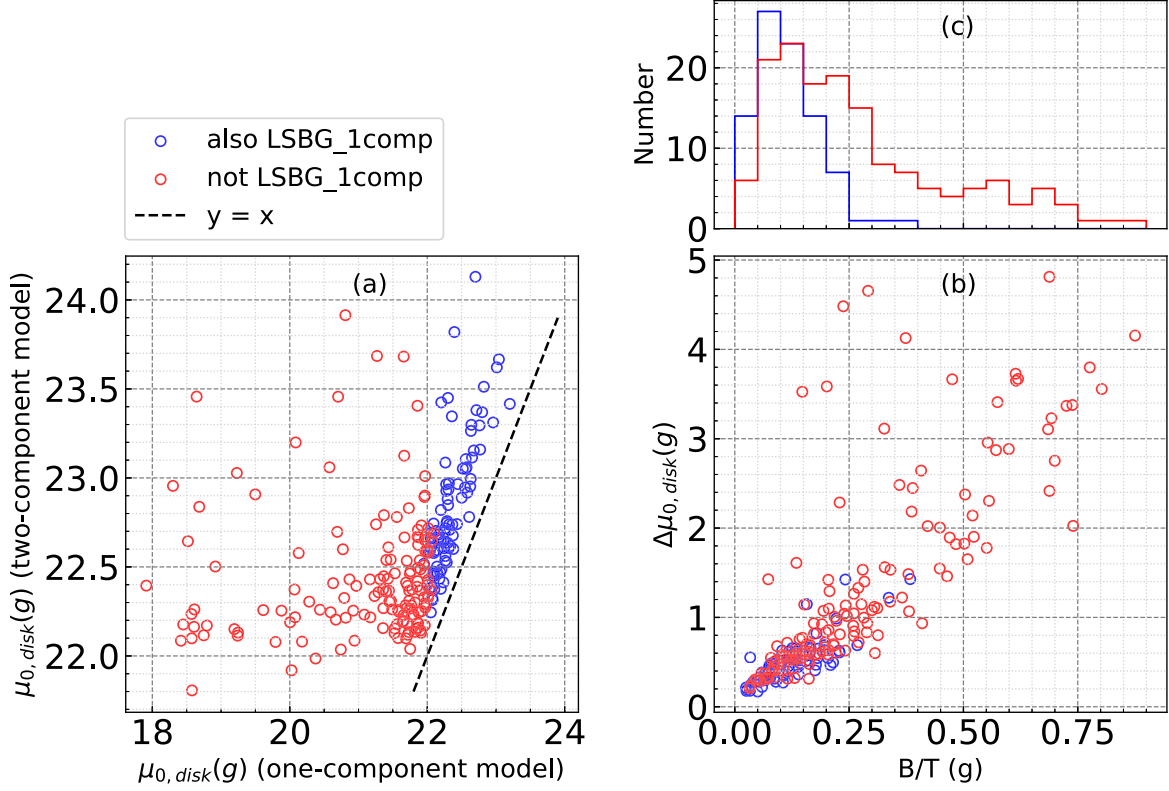
Figure 7. The difference of disk central surface brightness ($\mu_{0,\mathrm{disk}}$) derived from one-component model fitting and two-component model fitting. Among the 247 galaxies in LSBG_2comps, 88 of them are identified as LSBGs by the single-component fitting (blue, denoted as "also LSBG_1comp"), and 151 galaxies are not (red, denoted as "not LSBG_1comp"). The black dashed line is the one-to-one line. All the μ_0 values from two-component model fitting are dimmer than those from single-component model fitting, and the μ_0 difference is related to the bulge-to-total ratio(B/T) of the galaxy. More than 60% of our LSBG_2comps will not be selected by a single-component fitting, especially for the galaxies with larger B/T.

Table 5
Criteria for gLSBG Selection

Criterion	Reference
$\mu_{0,B} + 5 \times \log10(R_{s,B}) > 27.0$	Sprayberry et al. (1995)
$M_{\mathrm{H\,I}} > 10^9 M_\odot$ and $M_\star > 10^{10} M_\odot$	Honey et al. (2018)
$M_{\mathrm{H\,I}} \geqslant 10^{10} M_\odot$	O'Neil et al. (2023)
$R_s > 10$ kpc	Impey & Bothun (1997)
$R_{\mathrm{iso},28B} > 50$ kpc or $4R_s > 50$ kpc	Saburova et al. (2023)

of selection criteria. The first is the "diffuseness index" criterion proposed by Sprayberry et al. (1995): $\mu_{0,B} + 5 \times \log10(R_{s,B}) > 27.0$ where the scale length is in units of h^{-1} kpc. The second is the mass criterion: Honey et al. (2018) (hereafter H18) selected 41 gLSBGs from their spiral LSBGs with the criteria $M_{\mathrm{H\,I}} > 10^9 M_\odot$ and $M_\star > 10^{10} M_\odot$; O'Neil et al. (2023) adopted $M_{\mathrm{H\,I}} \geqslant 10^{10} M_\odot$ to identify massive LSBGs. The third is the size criterion: Impey & Bothun (1997) claimed that gLSBGs have scale lengths in excess of 10 kpc; Saburova
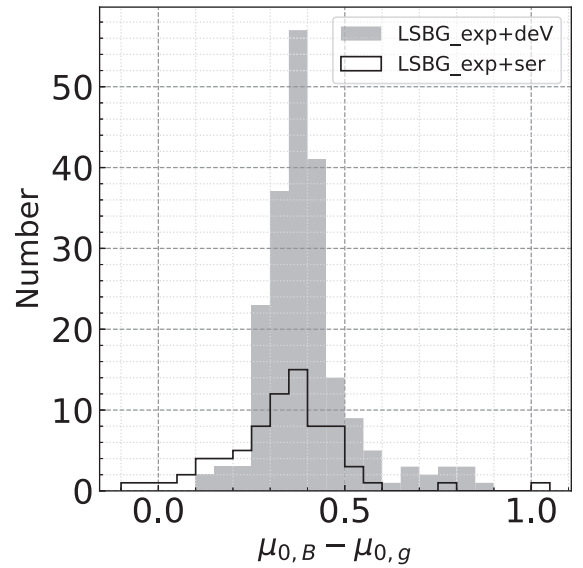
Figure 8. The histogram of the μ_0 difference between B and g band for LSBG_exp+deV and LSBG_exp+ser samples.

Table 6
Parameters of gLSBGs

AGCNr	R.A. (J2000)	Decl. (J2000)	$g-r$ (mag)	M_g (mag)	log(H I) ($M_\odot$)	log($M_\star$) ($M_\odot$)	$R_{s,g}$ (kpc)	$\mu_{0,g}$ (mag arcsec^{-2})	$n_{b,g}$	criterion
8848	209.014	13.506	0.743	−21.421	10.130	10.912	10.088	22.235	4.000	mass, size; exp+deV
9094	213.121	24.636	0.650	−21.628	10.640	10.851	9.486	22.114	4.000	mass; exp+deV
12 283	344.832	24.107	0.700	−21.426	9.810	10.847	8.643	22.086	4.000	mass; exp+deV
250883	232.229	7.745	0.698	−21.397	9.950	10.833	9.352	22.189	7.947	mass; exp+ser
210290	170.720	27.584	0.761	−21.085	10.000	10.807	11.609	23.457	4.000	diffuse, mass, size; exp+deV
201695	164.286	14.925	0.781	−20.837	10.150	10.738	6.611	22.131	4.000	mass; exp+deV
9654	225.236	11.517	0.720	−21.032	9.980	10.721	6.841	21.919	4.000	mass; exp+deV
4364	125.603	25.509	0.656	−21.252	9.990	10.709	9.041	22.078	4.000	mass; exp+deV
170281	119.332	11.206	0.627	−21.261	10.090	10.669	9.840	22.087	4.000	mass; exp+deV
241379	211.430	25.231	0.727	−20.866	9.940	10.665	4.777	22.171	4.000	mass; exp+deV
9491	221.061	4.219	0.656	−21.053	10.030	10.630	10.374	22.395	4.000	diffuse, mass, size; exp+deV
6072	164.935	10.071	0.610	−21.200	10.420	10.618	7.825	22.373	4.000	mass; exp+deV
213794	168.103	7.495	0.744	−20.579	10.280	10.578	8.209	22.151	4.454	mass; exp+ser
726722	218.947	24.753	0.780	−20.435	10.350	10.577	5.667	23.028	4.000	mass; exp+deV
749465	207.177	25.757	0.618	−20.958	10.440	10.533	8.160	22.305	4.000	mass; exp+deV
12 289	344.923	24.075	0.572	−21.127	10.300	10.528	9.133	22.709	4.000	diffuse, mass; exp+deV
714500	225.195	8.144	0.739	−20.420	10.070	10.507	5.231	22.177	4.000	mass; exp+deV
220208	183.279	16.086	0.767	−20.267	9.640	10.488	3.396	22.163	4.000	mass; exp+deV
251377	239.508	14.964	0.559	−20.926	10.400	10.428	7.391	22.036	4.000	mass; exp+deV
194959	141.762	27.845	0.652	−20.340	10.190	10.339	10.657	22.956	3.294	diffuse, mass, size; exp+ser
227546	192.794	26.795	0.668	−20.260	10.310	10.332	4.788	22.261	4.000	mass; exp+deV
220363	184.851	12.301	0.642	−20.337	9.680	10.321	6.062	22.145	4.000	mass; exp+deV
…	…	…	…	…	…	…	5.762	21.986	1.661	mass; exp+ser
9015	211.485	9.026	0.582	−20.421	10.020	10.261	7.884	22.442	4.000	mass; exp+deV
…	…	…	…	…	…	…	6.913	22.099	1.542	mass; exp+ser
731922	181.449	24.116	0.496	−20.674	10.370	10.230	10.026	22.502	1.697	diffuse, mass, size; exp+ser
240131	212.341	8.907	0.631	−20.099	9.760	10.210	4.699	22.260	4.000	mass; exp+deV
12 845	358.924	31.900	0.562	−20.355	10.180	10.205	9.202	22.433	4.000	mass; exp+deV
267940	240.576	12.274	0.710	−19.749	10.180	10.193	8.557	22.644	4.000	mass; exp+deV
123168	40.333	29.147	0.524	−20.368	9.920	10.151	6.708	22.093	4.000	mass; exp+deV
…	…	…	…	…	…	…	6.720	22.098	4.271	mass; exp+ser
211340	177.467	6.668	0.703	−19.664	9.350	10.147	3.238	22.838	4.000	mass; exp+deV
2197	40.858	31.471	0.525	−20.342	9.920	10.141	5.520	22.039	4.000	mass; exp+deV
194441	137.940	27.659	0.487	−20.249	9.870	10.044	6.336	22.134	4.000	mass; exp+deV
102667	11.070	25.766	0.403	−19.598	9.970	9.655	6.255	23.685	1.709	diffuse; exp+ser
190796	137.776	13.122	0.340	−19.836	10.140	9.651	8.407	23.199	2.210	diffuse; exp+ser
238684	195.473	5.387	0.304	−19.316	9.990	9.387	8.255	23.086	1.719	diffuse; exp+ser
258324	234.036	5.793	0.343	−18.765	9.720	9.227	7.103	23.718	4.000	diffuse; exp+deV
…	…	…	…	…	…	…	7.166	23.381	2.862	diffuse; exp+ser
102674	12.310	25.294	0.219	−19.168	10.020	9.195	7.633	23.566	4.000	diffuse; exp+deV
…	…	…	…	…	…	…	7.316	23.264	1.526	diffuse; exp+ser
749508	244.915	25.563	0.346	−18.541	9.820	9.143	8.117	24.429	4.000	diffuse; exp+deV
188781	132.116	16.192	0.397	−17.625	9.460	8.855	4.724	24.130	4.000	diffuse; exp+deV
202264	152.444	12.082	0.268	−17.802	9.650	8.726	6.468	23.819	1.676	diffuse; exp+ser

Note. The table is sorted by the g band stellar mass (log($M_\star$)). The last 8 galaxies have stellar mass smaller than $10^{10}M_\odot$, and all of them are selected by the "diffuseness index" criterion. They seem different from the gLSBGs that most people know, more like normal LSBGs with bulge. We will eliminate these 8 galaxies from our gLSBGs sample.

et al. (2023) (hereafter S23) detected 42 gLSBGs with $R_{\mathrm{iso},28B} > 50$ kpc or four times scale-length $4R_s > 50$ kpc.

This work will use these three kinds of criteria to select gLSBGs from our LSBG_2comps. Figure 8 shows that the μ_0 difference between B and g bands in our sample is ~ 0.35 mag arcsec^{-2}, so we adopt "diffuseness index"

$\mu_{0,g} + 5 \times \log 10(R_{s,g}) > 26.65$ and select a sample named "gLSBG_diffuse" which contains seven gLSBGs from LSBG_exp+deV and eight gLSBGs from LSBG_exp+ser with two galaxies replicated. Following the mass criterion in H18, we select a sample named "gLSBG_mass" which contains 27 gLSBGs from LSBG_exp+deV and seven
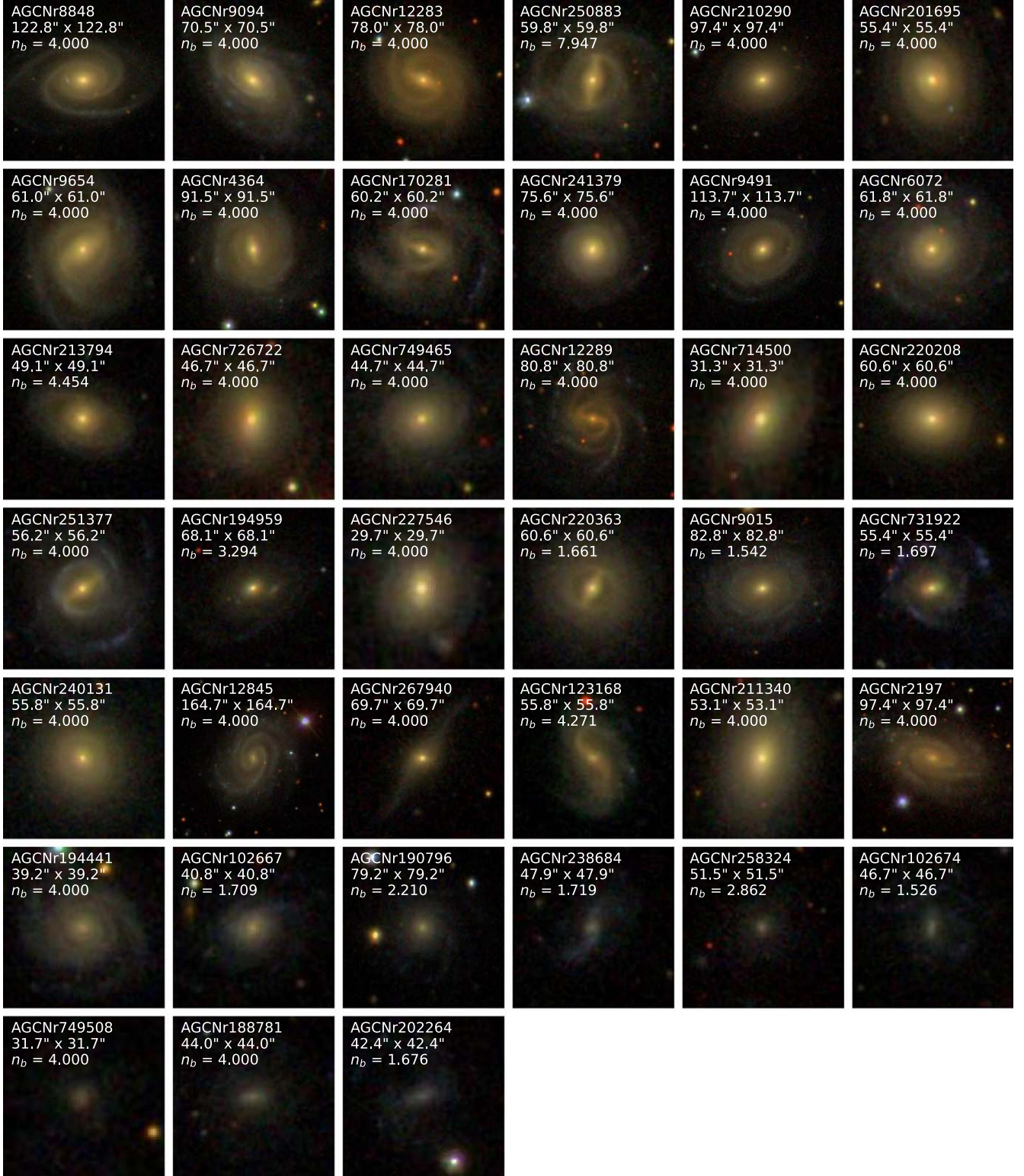
Figure 9. The colored images from SDSS of the gLSBGs. The first 31 galaxies are the gLSBGs whose stellar mass is larger than $10^{10} M_\odot$, and the last 8 galaxies are the gLSBGs whose stellar mass is smaller than $10^{10} M_\odot$. The last 8 galaxies seem different from the gLSBGs that most people know, more like normal LSBGs with bulge. We will eliminate these 8 galaxies from our gLSBGs sample.
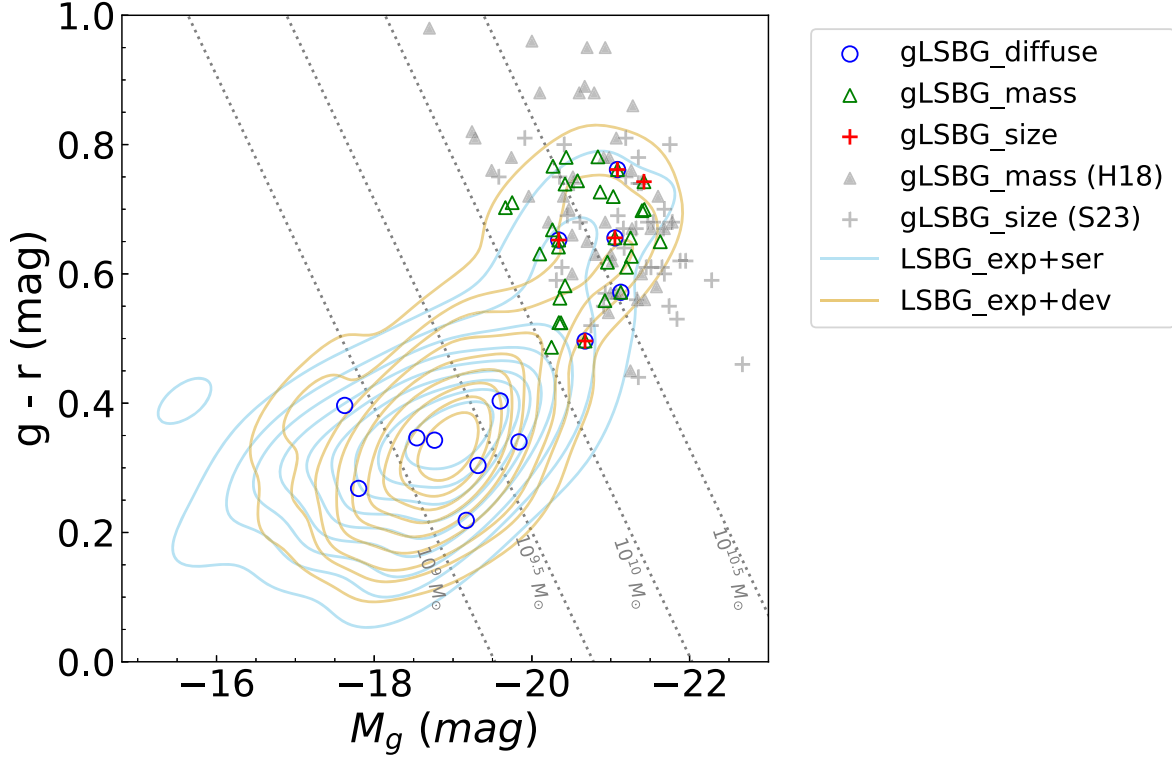
Figure 10. The color–magnitude diagram of gLSBGs superimposed on kernel density estimation (KDE) of LSBG_exp+deV (light yellow) and LSBG_exp+ser (light blue). Different shapes of marker represent the gLSBGs selected from different criteria. The gray triangles and gray crosses represent gLSBGs from H18 and S23, respectively. The gray dotted lines represent specific stellar mass values.

gLSBGs from LSBG_exp+ser with three galaxies replicated. We also select a sample named "gLSBG_size" under the criterion $R_{s,g} \geqslant 10$ kpc which contains three galaxies from LSBG_exp+deV and two gLSBGs from LSBG_exp+ser with no galaxy replicated. There are in total 39 non-repetitive gLSBGs, with detailed information listed in Table 6, and the SDSS color images of them are shown in Figure 9.

Figure 10 shows the color–magnitude diagram of gLSBGs superimposed on kernel density estimation (KDE) of LSBG_exp+deV (light yellow) and LSBG_exp+ser (light blue). The gray triangles and gray crosses represent gLSBGs from H18 and S23, respectively. The gray dotted lines represent stellar mass of $10^9 M_\odot$, $10^{9.5} M_\odot$, $10^{10} M_\odot$, and $10^{10.5} M_\odot$. Different shapes of marker represent the gLSBGs selected from different criteria. Among our 39 non-repetitive gLSBGs, 31 of them lie on the right side of the $10^{10} M_\odot$ stellar mass line. 90.32% (28/31) out of the 31 gLSBGs have the sérsic n index of the bulge component $n_b > 2$, indicating most of our gLSBGs hold a classical bulge. These 31 gLSBGs are located in the same region as gLSBGs in H18 and S23, they also seem similar to the gLSBGs that most people recognized which are red in color and giant in luminosity, mass, and size. There are eight galaxies on the left side of the $10^{10} M_\odot$ stellar mass line, and all these gLSBGs are selected by the "diffuseness index" criterion. They seem different from the

gLSBGs that most people know, more like normal LSBGs with bulge. This is because the dim $\mu_{0,disk}$ contributes a lot to the "diffuseness index". The median value of $\mu_{0,disk}$ of these eight gLSBGs is ~ 1.356 mag arcsec^{-2} dimmer than that of the 31 gLSBGs whose stellar mass is larger than $10^{10} M_\odot$. This is the drawback of the "diffuseness index" criterion. We will eliminate these eight galaxies from our gLSBGs sample. Our result suggests that for gas-rich LSBGs, $M_\star > 10^{10} M_\odot$ is a good criterion to distinguish between gLSBGs and normal LSBGs with bulge.

5. Summary

In this work, we carried out fitting of four models, exponential, sérsic, exp+deV, and exp+ser, to check the systematic effect in selecting LSBGs. Our parent sample is all the galaxies in $\alpha.40$ SDSS DR7 sample, and the images we used are the SDSS images after background reestimation (Du15). We took photometry and two-dimensional fitting for these images.

According to the criteria that the B band central surface brightness of the disk component $\mu_{0,disk}(B) \geqslant 22.5$ mag arcsec^{-2} and the axis-ratio of the disk component $b/a > 0.3$, we selected 1105, 1038, 207, and 75 none-edge-on LSBGs from each of the models. Because our parent sample is rich in H I gas, most of

our LSBGs are blue. The LSBGs selected by sérsic fitting are in principle the same type of galaxies as exponential fitting. LSBG_exp and LSBG_sérsic have 756 galaxies (68.42% of LSBG_exp and 72.83% of LSBG_sérsic) in common, the rest of the discrepancy is due to the difference between the exponential and sérsic models in obtaining μ_0. When $0.5 \leqslant n \leqslant 1.5$, the relation of μ_0 obtained from sérsic and exponential models can be written as $\mu_{0,\text{sérsic}} - \mu_{0,\text{exp}} = -1.34(n - 1)$. There are 1546 non-repetitive LSBGs, at least 15.89% of them hold a bulge. The galaxies in LSBG_2comps have larger disk, luminosity, and mass than galaxies in LSBG_1comp. But the bulges are not prominent in the majority of our LSBGs. More than 60% of the galaxies in LSBG_2comps will not be selected if we adopt a single disk model only. We also identified 31 non-repetitive gLSBGs, with 90.32% of them holding a classical bulge. They are located at the same region in the color–magnitude diagram as normal gLSBGs in literature. Based on our gas-rich LSBGs, we find $M_\star > 10^{10} M_\odot$ is a good criterion to distinguish between gLSBGs and normal LSBGs with bulge after we compared three kinds of criteria.

Acknowledgments

ORCID iDs

Bing-qing Zhang https://orcid.org/0000-0002-6659-1152
Hong Wu https://orcid.org/0000-0002-4333-3994
Wei Du https://orcid.org/0000-0003-4546-8216
Pin-song Zhao https://orcid.org/0000-0002-4328-538X
Min He https://orcid.org/0000-0001-6139-7660
Feng-jie Lei https://orcid.org/0000-0003-0408-5497

References

Abazajian, K. N., Adelman-McCarthy, J. K., Agüeros, M. A., et al. 2009, ApJS, 182, 543
Adelman-McCarthy, J. K., Agüeros, M. A., Allam, S. S., et al. 2006, ApJS, 162, 38
Adelman-McCarthy, J. K., Agüeros, M. A., Allam, S. S., et al. 2008, ApJS, 175, 297
Bertin, E., & Arnouts, S. 1996, A&AS, 117, 393
Bothun, G. D., Impey, C. D., Malin, D. F., & Mould, J. R. 1987, AJ, 94, 23
Brown, W. R., Geller, M. J., Fabricant, D. G., & Kurtz, M. J. 2001, AJ, 122, 714
Burkholder, V., Impey, C., & Sprayberry, D. 2001, AJ, 122, 2318
Cao, T.-W., Wu, H., Du, W., et al. 2017, AJ, 154, 116
Capaccioli, M. 1989, in World of Galaxies (Le Monde des Galaxies), ed. J. Corwin, G. Harold, & L. Bottinelli (New York: Springer), 208
Courteau, S. 1996, ApJS, 103, 363
de Blok, W. J. G., McGaugh, S. S., & van der Hulst, J. M. 1996, MNRAS, 283, 18
de Blok, W. J. G., van der Hulst, J. M., & Bothun, G. D. 1995, MNRAS, 274, 235
Dey, A., Schlegel, D. J., Lang, D., et al. 2019, AJ, 157, 168
Du, W., Cheng, C., Zheng, Z., & Wu, H. 2020, AJ, 159, 138
Du, W., Wu, H., Lam, M. I., et al. 2015, AJ, 149, 199
Fisher, D. B., & Drory, N. 2008, AJ, 136, 773
Galaz, G., Herrera-Camus, R., Garcia-Lambas, D., & Padilla, N. 2011, ApJ, 728, 74
Galaz, G., Milovic, C., Suc, V., et al. 2015, ApJL, 815, L29
Giovanelli, R., Haynes, M. P., Kent, B. R., et al. 2005, AJ, 130, 2598
Greco, J. P., Greene, J. E., Strauss, M. A., et al. 2018, ApJ, 857, 104
Hagen, L. M. Z., Seibert, M., Hagen, A., et al. 2016, ApJ, 826, 210
Haynes, M. P., Giovanelli, R., Martin, A. M., et al. 2011, AJ, 142, 170
He, M., Wu, H., Du, W., et al. 2020, ApJS, 248, 33
He, Y. Q., Xia, X. Y., Hao, C. N., et al. 2013, ApJ, 773, 37
Honey, M., van Driel, W., Das, M., & Martin, J. M. 2018, MNRAS, 476, 4488
Huang, S., Haynes, M. P., Giovanelli, R., et al. 2014, ApJ, 793, 40
Hyde, J. B., & Bernardi, M. 2009, MNRAS, 394, 1978
Impey, C., & Bothun, G. 1997, ARA&A, 35, 267
Kron, R. G. 1980, ApJS, 43, 305
Lauer, T. R., Faber, S. M., Richstone, D., et al. 2007, ApJ, 662, 808
Lei, F.-J., Wu, H., Du, W., et al. 2018, ApJS, 235, 18
Lei, F.-J., Wu, H., Zhu, Y.-N., et al. 2019, ApJS, 242, 11
Liang, Y. C., Zhong, G. H., Hammer, F., et al. 2010, MNRAS, 409, 213
Liu, F. S., Xia, X. Y., Mao, S., Wu, H., & Deng, Z. G. 2008, MNRAS, 385, 23
Martin, G., Kaviraj, S., Laigle, C., et al. 2019, MNRAS, 485, 796
McGaugh, S. 1996, in New Light on Galaxy Evolution, ed. R. Bender & R. L. Davies, Vol. 171 (Dordrecht: Springer), 97
McGaugh, S. S., & Bothun, G. D. 1994, AJ, 107, 530
McGaugh, S. S., Bothun, G. D., & Schombert, J. M. 1995a, AJ, 110, 573
McGaugh, S. S., Schombert, J. M., & Bothun, G. D. 1995b, AJ, 109, 2019
Moore, L., & Parker, Q. A. 2006, PASA, 23, 165
O'Neil, K. 2004, AJ, 128, 2080
O'Neil, K., Bothun, G. D., & Cornell, M. E. 1997, AJ, 113, 1212
O'Neil, K., Schinnerer, E., & Hofner, P. 2003, ApJ, 588, 230
O'Neil, K., Schneider, S. E., van Driel, W., et al. 2023, AJ, 165, 263
Pahwa, I., & Saha, K. 2018, MNRAS, 478, 4657
Peng, C. Y., Ho, L. C., Impey, C. D., & Rix, H.-W. 2002, AJ, 124, 266
Peng, C. Y., Ho, L. C., Impey, C. D., & Rix, H.-W. 2010, AJ, 139, 2097
Pickering, T. E., Impey, C. D., van Gorkom, J. H., & Bothun, G. D. 1997, AJ, 114, 1858
Pizzella, A., Corsini, E. M., Sarzi, M., et al. 2008, MNRAS, 387, 1099
Rosenbaum, S. D., Krusch, E., Bomans, D. J., & Dettmar, R. J. 2009, A&A, 504, 807
Saburova, A. S., Chilingarian, I. V., Kulier, A., et al. 2023, MNRAS, 520, L85
Simard, L., Mendel, J. T., Patton, D. R., Ellison, S. L., & McConnachie, A. W. 2011, ApJS, 196, 11
Smith, J. A., Tucker, D. L., Kent, S., et al. 2002, AJ, 123, 2121
Sprayberry, D., Impey, C. D., Bothun, G. D., & Irwin, M. J. 1995, AJ, 109, 558
Tanoglidis, D., Drlica-Wagner, A., Wei, K., et al. 2021, ApJS, 252, 18
Trujillo, I., Aguerri, J. A. L., Cepa, J., & Gutiérrez, C. M. 2001, MNRAS, 321, 269
van der Hulst, J. M., Skillman, E. D., Smith, T. R., et al. 1993, AJ, 106, 548
Willmer, C. N. A. 2018, ApJS, 236, 47
York, D. G., Adelman, J., Anderson, J. E. J., et al. 2000, AJ, 120, 1579
Zhong, G. H., Liang, Y. C., Liu, F. S., et al. 2008, MNRAS, 391, 986